Navier-Stokes Simulation for Flow Past an Open Cavity

Deepak Om*
The Boeing Company, Seattle, Washington

A two-dimensional Navier-Stokes code was developed to simulate the flow past an open cavity. The code employs the split explicit predictor-corrector algorithm of MacCormack in conservation law form. The purpose was to examine the unsteadiness of the shear layer and obtain details of the flowfield. Cavity flow was simulated for two different cavity sizes as well as for two different ramp shapes. Comparison with a wind-tunnel experiment shows good agreement. Those flows that were observed to be steady in the experiment were also steady in the computation; those flows that exhibited unsteady behavior of the shear layer in the experiment were also unsteady in the computation. Computations also showed that the shear-layer stability depends very strongly on the shape of the aft ramp and, with a proper ramp shape, the effect of cavity size was negligible on the shear-layer stability. These conclusions, also in agreement with the experimental results, were very useful in designing the cavity shape for the Boeing 767-AOA airplane.

Introduction

THERE have been numerous experimental investigations of flows over open cavities. Rossiter[1] measured time-averaged and unsteady pressures for a series of rectangular cavities. He found that the unsteady pressures contained both random and periodic components. Spee[2] conducted wind-tunnel experiments on the unsteady flow over a cavity system at high subsonic speeds to understand the interaction between sound waves and two-dimensional transonic flows. Heller and Bliss[3] used a water table to simulate supersonic flow over open rectangular cavities and to explain the unsteady behavior of the shear layer. Franke and Carr[4] studied the effects of geometric modifications for reducing flow-induced pressure oscillations in shallow, open, two-dimensional, rectangular cavities. Ethembabaoglu[5] also examined various types of geometric modifications to reduce the amplitude of cavity oscillations. Rockwell and Naudascher[6,7] have presented a detailed review of self-sustaining oscillations of the flow past cavities.

Thus, extensive measurements exist to give a qualitative description of cavity-flow phenomena. However, numerical simulations of cavity flow have not received the same kind of attention. Borland[8] used Euler equations to predict the unsteady flow over a rectangular cavity. Hankey and Shang[9] obtained numerical solutions of the Navier-Stokes equations for an open cavity at supersonic speed.

The purpose of the present investigation was to conduct a numerical study of the cavity-flow phenomenon on a modified Boeing 767. The Boeing 767-AOA (Airborne Optical Adjunct) airplane currently in design includes a large cupola fairing on top of the fuselage to house two optical sensor devices. Each optical sensor resides in its own compartment, one forward and one aft. Each compartment has a viewing port on the side of cupola, which will be opened during the observation part of the mission (Fig. 1). Therefore, the external cupola air must flow past two large open cavities.

The intent here is to design a cavity configuration that would have acceptable aerodynamic, acoustic, and optical transmission characteristics. The thin, stable shear layer, which reattaches smoothly onto the aft ramp of the viewing port (good aerodynamic properties), is thought to result in good optical transmission properties for the sensor as well as a low acoustical noise level in the cavity. Experiments with a single cavity were performed under the sponsorship of the U.S. Army/Strategic Defense Command (SDC) in the Model Boeing Transonic Wind Tunnel facility for different cavity sizes and aft ramp shapes. A typical configuration is shown in Fig. 2. Experiments were performed both with and without lip blowing. The purpose of the present Navier-Stokes simulation was to demonstrate the capability of simulating such cavity flows and to obtain details of the mean flowfield to get an insight into the physics of the problem. This was done by simulating cavity flows at wind-tunnel conditions with and without lip blowing to investigate the unsteadiness of the shear layer. In the present paper, however, results with no blowing will be presented. At the present time the code is being used to analyze the full-scale configuration at flight condition. This full-scale configuration was chosen based on the most stable wind-tunnel configuration.

Analysis

A two-dimensional Navier-Stokes code, TEM367,[10] as modified in Ref. 11, was modified further to simulate cavity flows. Although three-dimensional Navier-Stokes codes are available that can be modified to simulate cavity flows, the cost of such an analysis would be extremely high. Also, the current computer storage capabilities limit the size of the mesh that can be used to resolve the complete flowfield. For these reasons, a two-dimensional analysis was chosen. The results obtained with this analysis could be compared with the two-dimensional U.S. Army/SDC/Boeing wind-tunnel test.

Solution Procedure

The differential equations used by the code to describe the mean flow are the time-dependent, compressible Navier-Stokes equations. The governing equations are solved using the split explicit predictor-corrector algorithm of MacCormack[12,13] in conservation law form for a nonorthogonal body-fitted computational mesh. The equations are marched in time using the time step that corresponds to the smallest cell size in the flowfield. The flowfield is divided into three mesh regions as shown in Fig. 2. This allows three fluid streams to be analyzed simultaneously. In the computational logic space, each region is rectangular and has a separate I-J indexing scheme. This technique of subdividing the flowfield into

---

Presented as Paper 86-2628 at the AIAA Aircraft Systems, Design and Technology Meeting, Dayton, OH, Oct. 20-22, 1986; received Sept. 30, 1987; revision received April 26, 1988.

*Senior Specialist Engineer. Member AIAA.

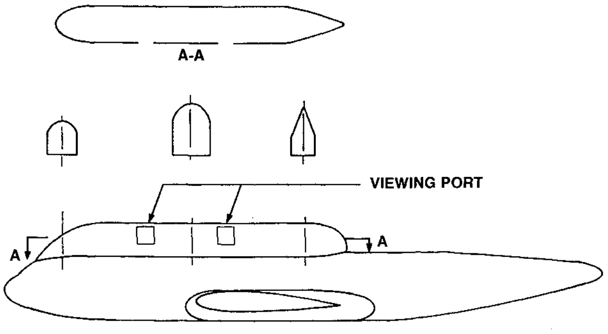

Fig. 1 Cupola fairing on top of 767 fuselage.

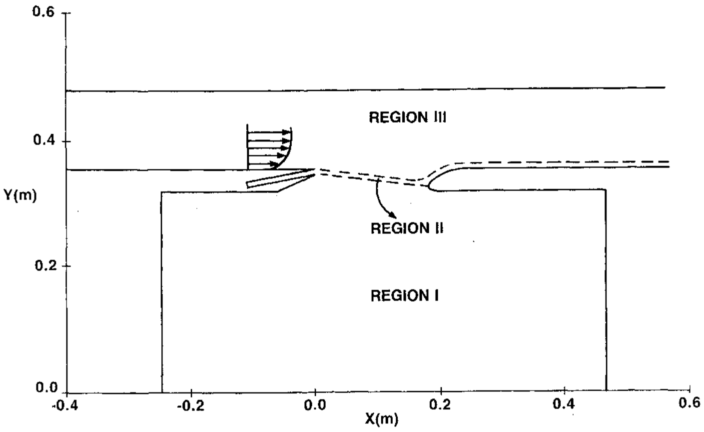

Fig. 2 Three regions of the flowfield.

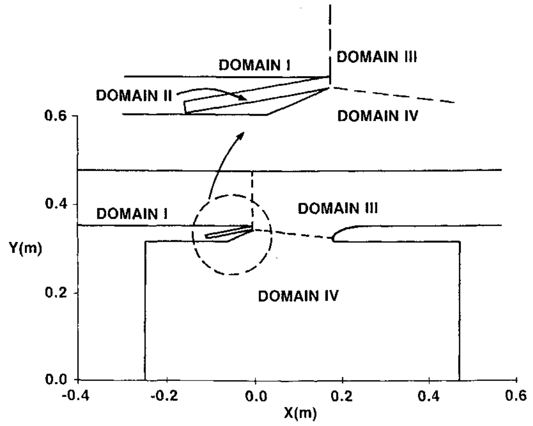

Fig. 3 Four domains for generating grids.

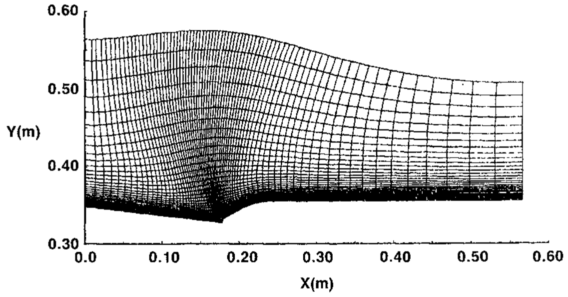

Fig. 4a Hyperbolic grid for domain III.

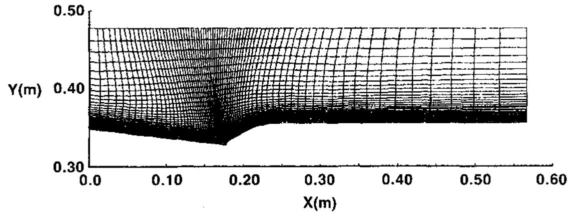

Fig. 4b Compressed grid for domain III.

several coupled computational regions conserves computer storage and eases mesh generation.

Grid Generation

In the original code, the I-mesh lines were vertical and parallel to the y-coordinate axis and the J-mesh lines were fitted to the body. The mesh system generated by this code resulted in highly sheared meshes near the edge of the aft ramp. The resultant truncation errors associated with these meshes caused the program to blow up in the region of sheared meshes. For this reason, it was decided to use a hyperbolic H-mesh to reduce mesh shearing.

The flowfield was divided into four domains (Fig. 3). Domains I and II used algebraic meshes with vertical I-mesh lines, whereas domains III and IV used hyperbolic meshes. A hyperbolic grid generator (developed by Larry Wigton of the Boeing Commercial Airplane Company) was used for domain III. The far-field boundary did not represent the wind-tunnel wall as desired (Fig. 4a). Therefore, each constant I-line was compressed algebraically such that the far-field boundary was a horizontal line representing the wind-tunnel wall (Fig. 4b). This, of course, loses orthogonality. Mesh was generated in a similar manner for domain IV and then compressed algebraically to represent the cavity floor. The first few meshes near the lower boundary of domain III are kept uniform in J-direction so that they can be matched with uniform domain II mesh. The mesh compression takes place in the region beyond the uniform meshes. All of the mesh lines are continuous at the domain boundaries.

Boundary Conditions

Boundary conditions are imposed using fictitious cells bordering the computational regions. At solid, impermeable boundaries, convection terms are explicitly zeroed to maintain strict mass conservation and a zero normal pressure gradient is assumed (no slip). The free-slip condition is prescribed for the far-field boundary or the wind-tunnel wall. A wall function boundary condition is used for the upstream boundary layer. Total pressure, total temperature, and flow angle are specified at subsonic inflow boundaries, with the remaining field variables obtained by using a one-dimensional method of characteristics. At the subsonic outflow boundary, pressure is prescribed. The remaining field variables are obtained by assuming a zero axial gradient in each variable. Since experimental pressure was not available at the downstream boundary, a few iterations were required to determine the downstream pressure such that the Mach number at the upstream boundary was close to the freestream value.

Wall Functions

Resolution of turbulent boundary layers requires the grid point closest to the solid boundary to be within the viscous sublayer. This makes the mesh near the boundary very small. The stability condition for the explicit method requires an exceedingly small time-step size. This drives the computation time prohibitively large. For this reason, wall functions are used to obtain the wall shear stresses and convective fluxes in the mesh cells near solid boundaries. This greatly reduces the number of mesh points required for turbulent boundary layers.

Turbulence Model

Algebraic eddy-viscosity turbulence models used in the code are described in detail in Ref. 10. A two-layer mixing-length model was used to describe the boundary layer. A simple mixing-length model was used to describe the shear layer in which the eddy viscosity is proportional to the thickness of the mixing layer and the difference between the tangential velocities across the layer. The mixing-layer thickness was assumed to vary linearly with downstream distance having an initial value equal to the upstream boundary-layer thickness.

When the shear layer reattaches itself on the aft ramp, the use of an algebraic eddy-viscosity turbulence model does not seem feasible for this complex region, where the length scale of turbulence must make the transition from a free shear layer to an attached boundary layer. The problem is the a priori specification of a length scale. An appropriate choice would be the use of a two-equation model that calculates its own length scale. Since the main interest of the present study was to study the shear-layer oscillation and not the redevelopment of the boundary layer, it was decided to use the existing algebraic turbulence model present in the code. Over the ramp surface, the eddy viscosity is computed using the boundary-layer model.

Smoothing Terms

In regions of low fluid velocity and particularly regions where there exist large second derivatives in the conservative field variables, the algorithm requires smoothing to prevent numerical instability. Explicit smoothers are added using the fourth-order pressure term introduced by MacCormack and Baldwin.[13] In addition, a linear diffusion term was included, which was used mainly to damp large transients generated by the initial conditions. The two smoothers are combined in a single term and added to each of the field equations.

Initial Conditions

Outside the cavity (region III of Fig. 2), the upstream condition is imposed everywhere. Inside the cavity (region I of Fig. 2), the flow is assumed to be static, i.e., $U = 0$, $V = 0$, $T = T_0$, and $P = P_\infty$. Region II (Fig. 2) flow is also assumed to be static.

The present code has a restart capability. The solution generated for a particular mesh may be used as the initial condition for subsequent computations involving the same mesh size but with a different CFL number or artificial viscosity coefficient.

Results and Discussion

This paper presents results of the Navier-Stokes analysis for three wind-tunnel cases, the data for which were made available by the U.S. Army/SDC. The freestream total pressure was 1 atm and the total temperature was 300 K. The cavity viewing port length is 0.1778 m (7.0 in.). M_∞ and δ, the thickness of the turbulent boundary layer, correspond to the upstream computational boundary. The three wind-tunnel cases are as follows:

I) 14×31 in. cavity size with a blunt ramp: $M_\infty \sim 0.65$, $\delta \sim 1.0$ in. (2.54 cm).

II) 11×17 in. cavity size with a blunt ramp: $M_\infty \sim 0.65$, $\delta = 1.0$ in. (2.54 cm).

III) 11×17 in. cavity size with a sharp ramp: $M_\infty \sim 0.65$, $\delta = 1.0$ in. (2.54 cm).

All of the computations were performed on a Cray X-MP machine. The number of cycles marched for each case is given in the respective subsections that follow.

Case I: 14 × 31 in. Cavity Size with a Blunt Ramp

The wind-tunnel test for this case showed a stable shear layer that reattached smoothly on the aft ramp, as can be seen from one of the schlieren pictures shown in Fig. 5a. Repeated schlieren pictures showed a very similar behavior.

The computational mesh system for this configuration, shown in Fig. 5b, employs a 90×31, 84×10, and 92×29 mesh for the three regions shown in Fig. 2. Every other grid point is plotted in both directions for Fig. 5b. The meshes in the streamwise direction were clustered near the aft ramp because large flow gradients were expected to occur near the ramp. A CFL number of 0.9 was used for this case as well as for all of the subsequent cases. The computation was marched in time for 22,000 cycles. It took about 0.11 s of CPU time per cycle.

Stagnation point location history is used to monitor the unsteadiness of the shear layer. The computation shows a stable shear layer (Fig. 5c). The stagnation point reaches an asymptotic value and agrees quite well with the experimental value obtained from the oil-flow picture.

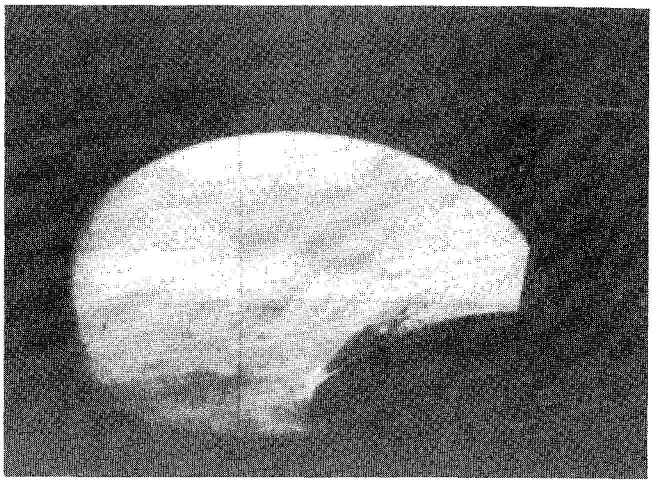

Fig. 5a Schlieren photograph of 14×31-in. cavity near a blunt ramp.

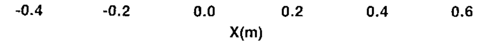

Fig. 5b Mesh system for 14×31-in. cavity with a blunt ramp.

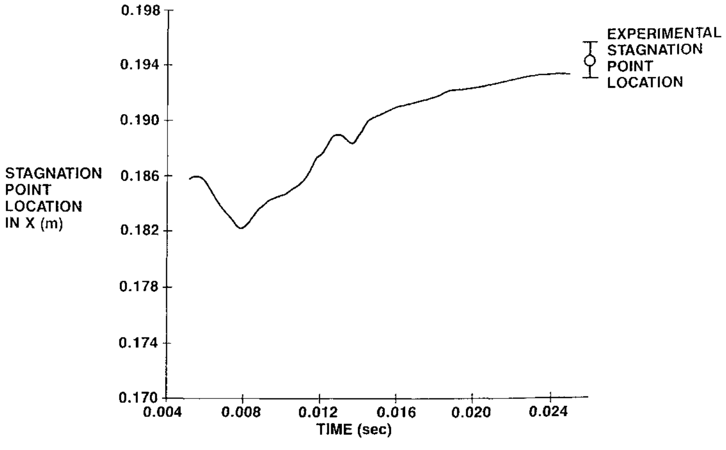

Fig. 5c Stagnation point history.

Velocity vectors at time = 20.48 ms are shown in Fig. 5d. The velocity vector plot shows a large recirculating flow near the aft ramp. Thus, mass is entrained into the cavity near the aft ramp, and it goes out of the cavity from the upstream end of its opening. This, in turn, causes a counterrotating flow in the right side of the cavity. This flow is responsible for producing the reversed flow underneath the ramp, which was also observed experimentally using the oil-flow technique.[14]

The Mach number contour at time = 20.48 ms is shown in Fig. 5e. The upstream boundary layer becomes a shear layer over the cavity and reattaches itself on the aft ramp. The proximity of the wind-tunnel wall to the cavity forms a channel over the ramp surface. The boundary layer downstream in this channel becomes much thicker, as expected. The other main features of the flow include the following: 1) very low Mach number flow in the cavity, and 2) an increased freestream Mach number in the downstream channel. With the displacement thickness buildup in the downstream channel, the effective area of the channel is reduced, which produces a higher Mach number flow.

The density contour at time = 20.48 ms is shown in Fig. 5f. It shows a steady shear layer reattaching smoothly onto the aft ramp, as was seen in the schlieren photograph (Fig. 5a).

This suggests that, by properly contouring the aft ramp shape, the shear layer can be made stable or the pressure oscillations in the shear layer can be reduced. Similar observations were made by Franke and Carr[4] and Ethembabaoglu[5] in their experimental investigations.

Case II: 11 × 17 in. Cavity Size with the Blunt Ramp

The wind-tunnel test for this case showed a stable shear layer, as can be seen from one of the schlieren pictures shown in Fig. 6a. Repeated schlieren pictures showed a very similar behavior.

The computational mesh system for this configuration, as shown in Fig. 6b, employs a 79 × 29, 84 × 10, and 92 × 29 mesh for the three regions. The computation was marched in time for 17,000 cycles. It took about 0.1044 s of CPU time per cycle. The computational results show a stable shear layer, as seen in Fig. 6c. The flow behaves very similar to the case I flow. Experimental stagnation point location was not available for this case as well as for the subsequent case. Mach number contours at time = 19.36 ms are shown in Fig. 6d.

Case III: 11 × 17 in. Cavity Size with a Sharp Ramp

This case is identical to case II except the blunt ramp is replaced with a sharp ramp. The wind-tunnel test for this case showed an unstable shear layer, as can be seen from one of the schlieren pictures shown in Fig. 7a. Repeated schlieren pictures showed an unsteady shear layer.

The computational mesh system for this configuration, as shown in Fig. 7b, employs 80 × 29, 84 × 10, and 92 × 29 mesh for the three regions. The computation was marched in time for 13,000 cycles. It took about 0.16 s of CPU time per cycle. The computational results show an unsteady shear layer, as can be seen from the stagnation point history (Fig. 7c). Stagnation point history (Fig. 7c) shows that the shear layer reattaches on the aft ramp but oscillates about a certain point on the ramp. Pressure histories at two points in the shear layer (Figs. 7d and 7e) also show the unsteady nature of the shear layer. The average pressure at P3R (Fig. 7d), which is near the stagnation point, is higher than the average pressure at P3L (Fig. 7e), as expected. The Mach number contour at time = 18.83 ms is shown in Fig. 7f.

A comparison of the Mach number contour (Fig. 7f) with the Mach number contour of the same cavity size but with a blunt ramp (Fig. 6d) shows that the Mach number inside the cavity is higher for the sharp ramp. This suggests that more mass is entrained into the cavity for the sharper ramp, which is probably responsible for inducing the shear-layer oscillation with successive mass expulsion from the cavity and mass entrainment into it.

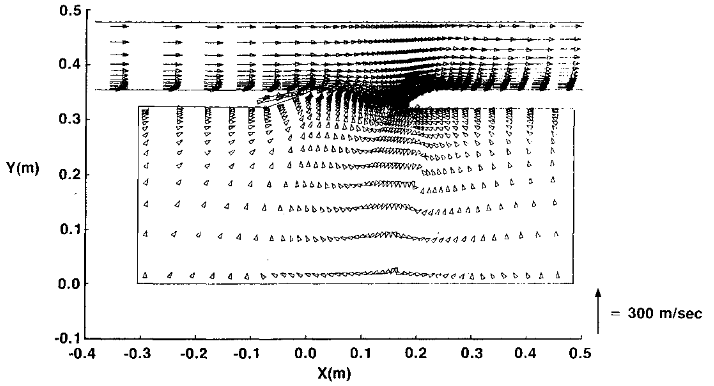

Fig. 5d **Velocity vectors at time = 20.48 ms.**

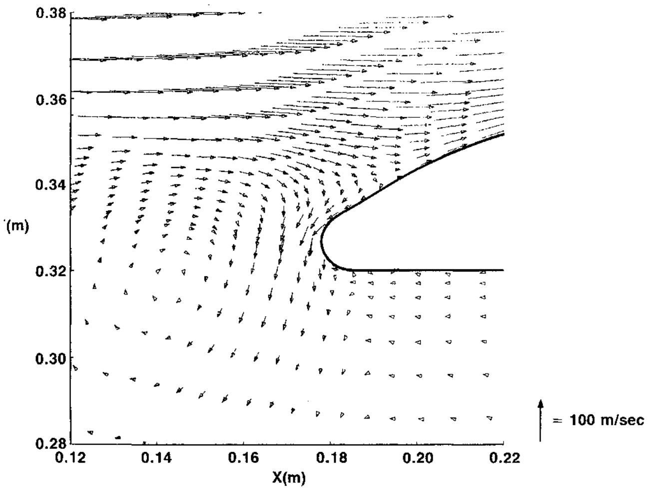

Fig. 5d (contd.) **Velocity vectors near the aft ramp at time = 20.48 ms.**

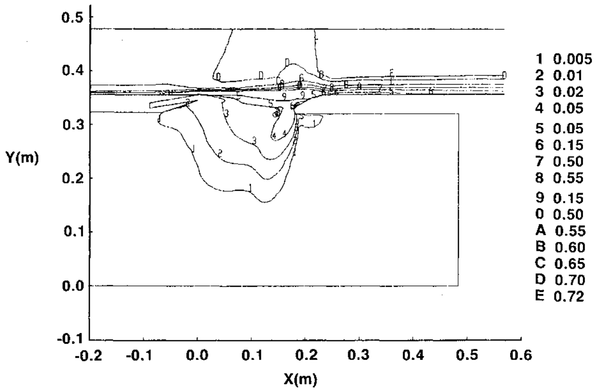

Fig. 5e **Mach number contours at time = 20.48 ms.**

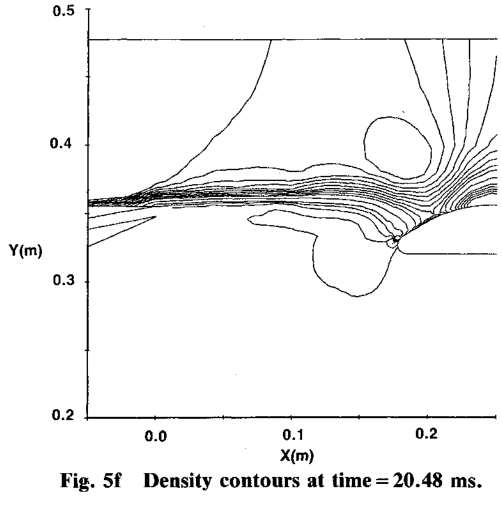

Fig. 5f **Density contours at time = 20.48 ms.**

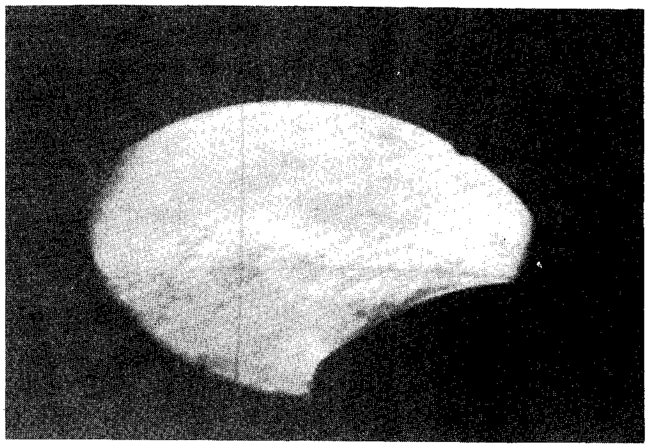

Fig. 6a Schlieren photograph of 11 × 17-in. cavity near a blunt ramp.

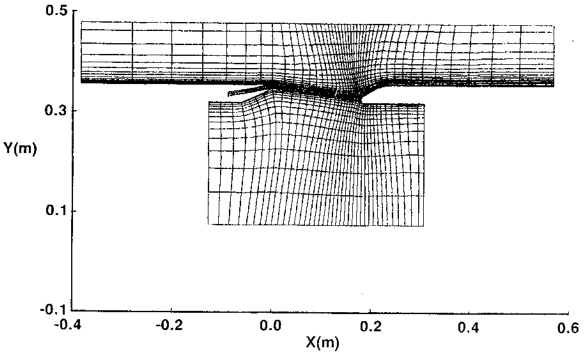

Fig. 6b Mesh system for 11 × 17-in. cavity with a blunt ramp.

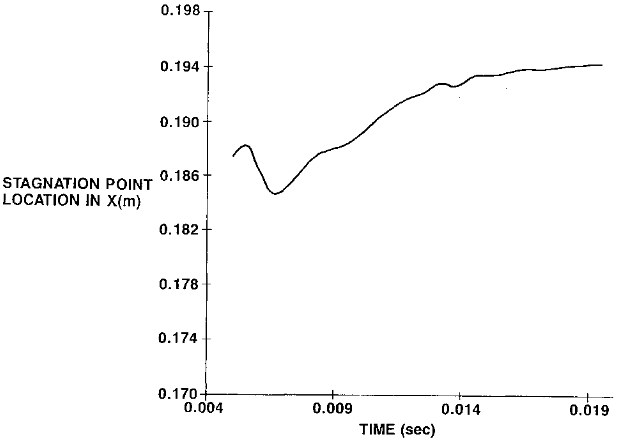

Fig. 6c Stagnation point history.

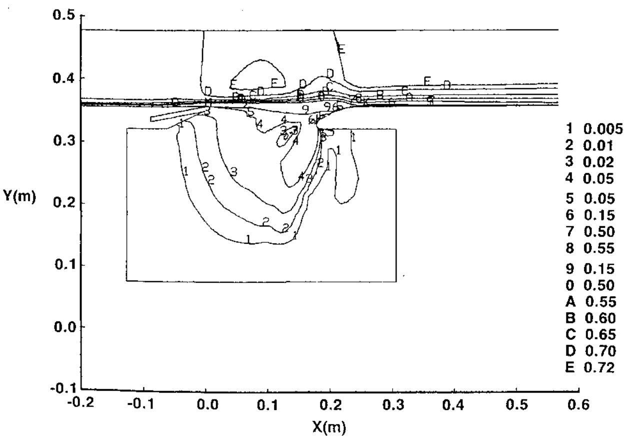

Fig. 6d Mach number contours at time = 19.36 ms.

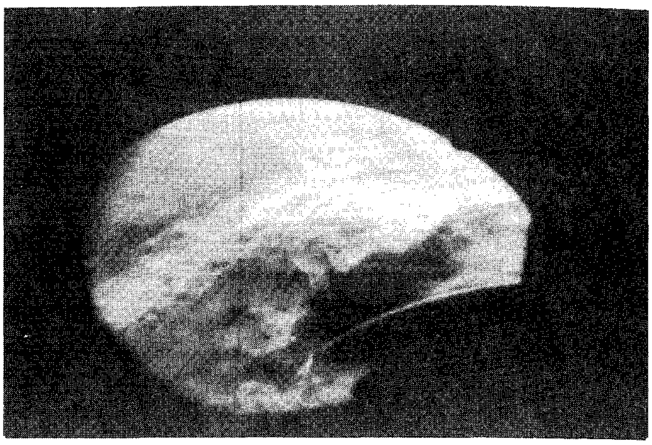

Fig. 7a Schlieren photograph of 11 × 17-in. cavity with a sharp ramp.

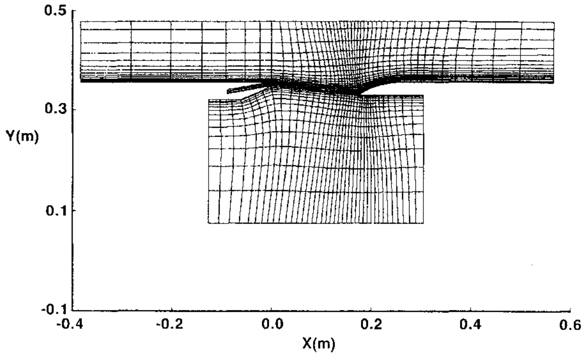

Fig. 7b Mesh system for 11 × 17-in. cavity with a sharp ramp.

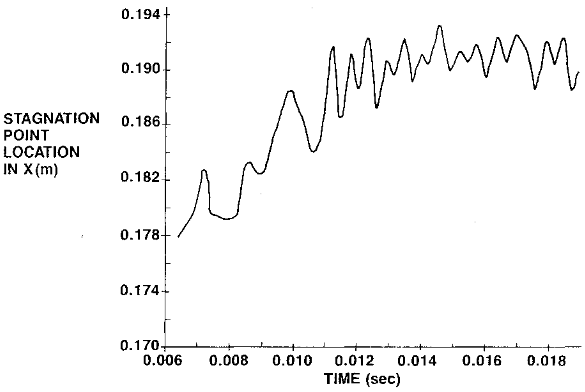

Fig. 7c Stagnation point history.

This is consistent with Spee's[2] observations from his wind-tunnel test. Spee mentions in his paper that periodical inflows and outflows take place, from the outer flow into the cavity and back, associated with the lateral displacement at the aft ramp, and caused by the fluctuating pressure difference between the inner and outer flows. This pressure difference in its turn is a consequence of the inflow and outflow. Spee also found visible variations of the stagnation point position on the aft ramp, which is consistent with the present numerical solution (Fig. 7c).

An important condition for the generation of shear-layer oscillations can be described in terms of an effective feedback. Spee[2] and Rockwell and Naudascher[6] give a good description of this mechanism. This feedback, which is essentially the upstream propagation of disturbances produced at the downstream cavity edge, produces vorticity fluctuations near the sensitive shear-layer origin, which, in turn, provide enhanced

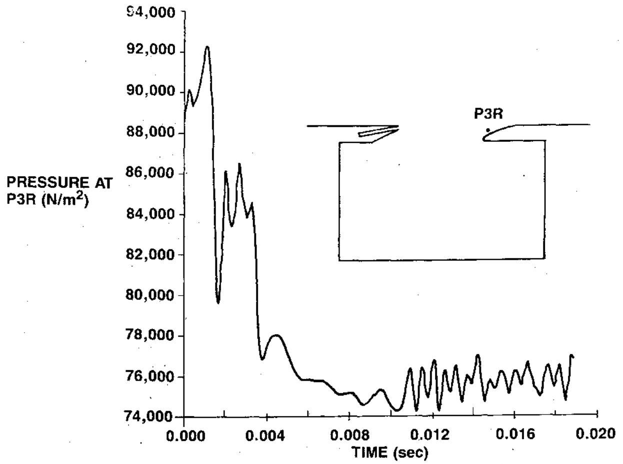

Fig. 7d Pressure history at point P3R.

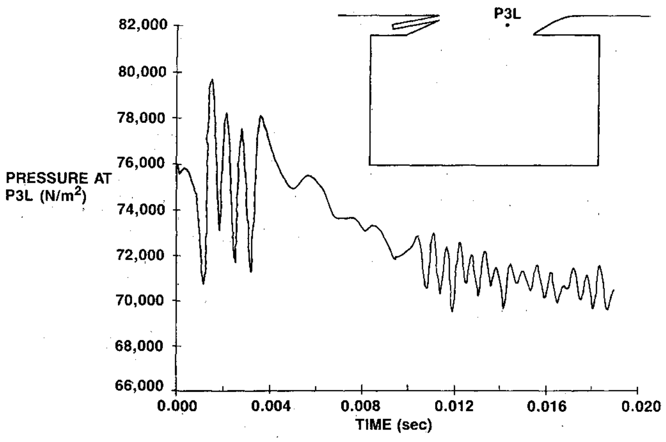

Fig. 7e Pressure history at point P3L.

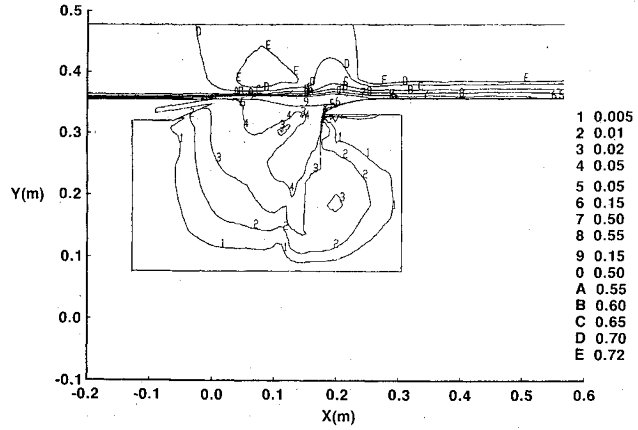

Fig. 7f Mach number contours at time = 18.83 ms.

disturbances to be amplified further in the shear layer, and so on.

The density contour, shown in Fig. 7g, clearly exhibits an unsteady behavior of the shear layer and qualitatively compares very favorably with the schlieren photograph of Fig. 7a.

Comment on Numerical Scheme

The split operators of MacCormack et al.,[12,13] which advance the solution from the n time level to the $n + 1$ time level, were not applied symmetrically in the original code.[10] The scheme is second-order accurate in space, but since the operators are not applied symmetrically, it is only first-order accurate in time. In the original code, only steady-state solutions were of interest; therefore, the lack of operator symmetry was incorporated. However, for unsteady flows, second-order accuracy in time is desirable. But, since low CFL values are used with the explicit method, time accuracy is somewhat retained. It is felt that this would be adequate for the present cavity problem since we are interested mainly in the qualitative definition of the shear-layer unsteadiness. However, in future endeavors it is advisable to apply the operators symmetrically to make the scheme second-order accurate in time.

It would be desirable to study the effect of mesh refinement in the normal direction over the aft ramp surface to see how well it resolves the boundary layer. This is needed since the wall function boundary condition was not used on the ramp surface.

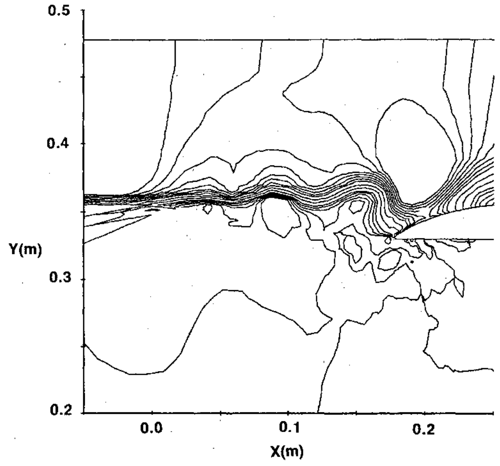

Fig. 7g Density contours at time = 18.83 ms.

Concluding Remarks

The numerical simulation of the Airborne Optical Adjunct (AOA) cavity flow using a two-dimensional Navier-Stokes code showed good qualitative agreement with the U.S. Army/SDC wind-tunnel test. It also provided details of the flowfield that were not available from the wind-tunnel test. The analysis of two different cavity sizes (14 × 31 in. and 11 × 17 in.) with a blunt ramp showed that the shear layer remained stable for both cases. When a sharp ramp was used in place of the blunt ramp with the 11 × 17 in. cavity size, the shear layer exhibited self-sustained oscillation. These results were in agreement with the wind-tunnel results. Based on these results, the cavity with the larger dimension (14 × 31 in.) and blunt ramp was chosen as the baseline configuration. A larger dimension of the cavity allows more room for the optical sensor.

Currently, the code is being used to analyze the full-scale cavity configuration for the 767-AOA airplane. This full-scale configuration was chosen based on the wind-tunnel baseline configuration. The intent is to find out if the shear layer, which was stable at the wind-tunnel condition, would remain stable at the flight condition. Also, the density contours obtained from the Navier-Stokes computation will be used to evaluate the optical transmission characteristics of the shear layer at the flight condition.

Acknowledgments

This computational work was funded by the Boeing Commercial Airplane Company. The author is thankful to the U.S. Army/SDC; to Dr. Mansop Hahn of Boeing Commercial Airplane Company for making available the experimental results; and to Edward Tinoco of Boeing Commercial Airplane Company for helpful discussions.

References

[1] Rossiter, J. E., "Wind Tunnel Experiments on the Flow Over Rectangular Cavities at Subsonic and Transonic Speeds," Aeronautical Research Council, R&M 3428, Oct. 1964.

[2] Spee, B. M., "Wind-Tunnel Experiments on Unsteady Cavity Flow at Subsonic Speeds," *Separated Flow II,* AGARD Conference Proceedings, Rhode-Saint-Genèse, Belgium, No. 4, May 1966.

[3] Heller, H. and Bliss, D., "Aerodynamically Induced Pressure Oscillations in Cavities: Physical Mechanisms and Suppresion Concepts," Wright-Patterson AFB, OH, Air Force Flight Dynamics Lab., TR-74-133, Feb. 1975.

[4] Franke, M. E. and Carr, D. L., "Effect of Geometry on Open Cavity Flow-Induced Pressure Oscillations," AIAA Paper 75-492, March 1975.

[5] Ethembabaoglu, S., "On the Fluctuating Flow Characteristics in the Vicinity of Gate Slots," Div. of Hydraulic Engineering, Univ. of Trondheim, Norwegian Inst. of Technology, June 1973.

[6] Rockwell, D. and Naudascher E., "Review—Self-Sustaining Oscillations of Flow Past Cavities," *Journal of Fluids Engineering,* Vol. 100, June 1978, pp. 152–165.

[7] Rockwell, D. and Naudascher, E., "Self-Sustained Oscillations of Impinging Free Shear Layers," *Annual Review of Fluid Mechanics,* 1979, pp. 67–94.

[8] Borland, C. J., "Numerical Prediction of the Unsteady Flowfield in an Open Cavity," AIAA Paper 77-673, June 1977.

[9] Hankey, W. L. and Shang, J. S., "Analyses of Pressure Oscillations in an Open Cavity," *AIAA Journal,* Vol. 18, Aug. 1980, pp. 892–898.

[10] Peery, K. M. and Forester, C. K., "Numerical Simulation of Multistream Nozzle Flows," *AIAA Journal,* Vol. 18, Sept. 1980.

[11] Campbell, A. F. and Syberg, J., "Design Study of an External Compression Supersonic Inlet Using a Finite-Difference Two-Dimensional Navier-Stokes Code," AIAA Paper 84-1275, June 1984.

[12] Hung, C. M. and MacCormack, R. W., "Numerical Solutions of Supersonic and Hypersonic Laminar Flows Over a Two-Dimensional Compression Corner," AIAA Paper 75-2, Jan. 1975.

[13] MacCormack, R. W. and Baldwin, B. S., "A Numerical Method for Solving the Navier-Stokes Equations with Application to Shock-Boundary Layer Interactions," AIAA Paper 75-1, Jan. 1975.

[14] Hahn, M. M., Private communication, Oct. 1985.